ACS APPLIED MATERIALS & INTERFACES

Research Article

www.acsami.org

Antioxidant and Antiradical SiO_2 Nanoparticles Covalently Functionalized with Gallic Acid

Yiannis Deligiannakis,*,† Georgios A. Sotiriou, and Sotiris E. Pratsinis

Particle Technology Laboratory, Institute of Process Engineering, Department of Mechanical and Process Engineering, ETH Zurich, Sonneggstrasse 3, 8092 Zurich, Switzerland

Supporting Information

ABSTRACT: Gallic acid (GA) and its derivatives are natural polyphenolic substances widely used as antioxidants in nutrients, medicine and polymers. Here, nanoantioxidant materials are engineered by covalently grafting GA on SiO_2 nanoparticles (NPs). A proof-of-concept is provided herein, using four types of well-characterized SiO_2 NPs of specific surface area (SSA) 96−352 m^2/g. All such hybrid SiO_2-GA NPs had the same surface density of GA molecules (~1 GA per nm^2). The radical-scavenging capacity (RSC) of the SiO_2-GA NPs was quantified in comparison with pure GA based on the 2,2-diphenyl-1-picrylhydrazyl ($DPPH^•$) radical method, using electron paramagnetic resonance (EPR) and UV−vis spectroscopy. The scavenging of DPPH radicals by these nanoantioxidant SiO_2-GA NPs showed mixed-phase kinetics: An initial fast-phase ($t_{1/2}$ <1 min) corresponding to a H-Atom Transfer (HAT) mechanism, followed by a slow-phase attributed to secondary radical−radical reactions. The slow-reactions resulted in radical-induced NP agglomeration, that was more prominent for high-SSA NPs. After their interaction with DPPH radicals, the nanoantioxidant particles can be reused by simple washing with no impairment of their RSC.

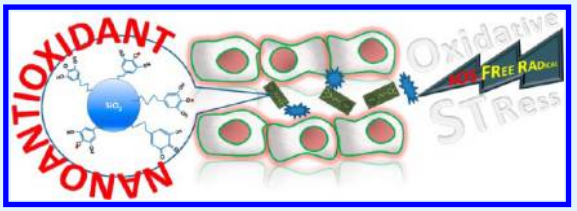

KEYWORDS: *nanoantioxidant, DPPH radical, gallic acid, grafting, nanoparticle, agglomeration*

INTRODUCTION

Antioxidants preventing free-radical reactions attract intense scientific and economic interest in human health,[1,2] food,[3] and polymer[4] industries. Antioxidants, at low concentrations, delay or prevent molecular deterioration by adverse radical reactions and radical-related oxidation[1−3] and protect the human body against damage by reactive oxygen species.[1] Food-industry, (see review in ref 4 and references therein) aims to minimize radical-induced deterioration (e.g., rancidity) using antioxidants during the manufacturing process.[4] That way, foods can maintain their nutritional quality over a defined shelf life.[5] To minimize polymer oxidative degradation, researchers also added anti-oxidants to polymers in small amounts.[4]

Among natural antioxidants, polyphenols successfully scav-enge free radicals via their OH groups.[6] There is a high correlation between content of phenolic substances and total antioxidant activity of various plant extracts.[7,8] Currently, gallic acid (GA, 3,4,5-trihydroxybenzoic acid) and its derivatives, are regularly applied in pharmaceutical[9] and food industry.[10] GA derivatives are exploited in phytomedicine, for example, as free radical scavengers,[11] inducing apoptosis of cancer cells,[12−14] and interfering with the signal pathways involving Ca^{2+} and oxygen radicals.[15−17] Traditional stabilizers for polyolefins are typically based on a phenolic antioxidant.[4]

Currently, major challenges faced in the antioxidants' technology are

(i) Eliminating deactivation of polyphenolic antioxidants via oxidation under ambient O_2[18−20] and polymerization, e.g., polyphenols' browning,[21,22] which restricts its lifetime within minutes. This mechanism has been investigated in full detail for GA in aqueous solution.[23]
(ii) Minimization of leaching and eventual volatilization of the antioxidant. This is most relevant to food-packaging and polymer-related technologies.[24−26]
(iii) Controlling the thermal stability, and therefore the lifetime, of the antioxidant. In food-packaging and polymers, during thermal treatment even at mild temperatures, such as sterilization or pasteurization, peroxide radicals[1,3] are generated that cause bond scission in polymers. This has been clearly proven to cause scission of the polyethylene backbone.[27]

In natural systems, these challenges (i−iii) have been successfully addressed by (a) sequestration of the antioxidant in a matrix which can be a protein, carbohydrate or lipid, and (b) preventing undesired radical−radical couplings.[28,29] During the last 5 years, incorporation of natural antioxidants in material-matrices is exploited as advanced technology to overcome the drawbacks detailed in (i−iii). Pertinent examples, where GA was used to functionalize organic polymers, are chitosan[30,31] and gelatin.[32] Other relevant antioxidant-polymers reported are caffeic acid-functionalized chitosan[33] and poly-propylene.[34] In an alternative approach, inorganic materials can be exploited for this purpose. For example, a commercial montmorillonite clay (Laponite), can be used to stabilize

Received: August 22, 2012
Accepted: November 2, 2012
Published: November 2, 2012

Table 1. Specific Surface Area (SSA), GA Loading, and GA Radical Concentration for the SiO_2-GA NPs

				GA surface concentration (μM/gram)		GA surface density	
material	SSA (m^2/g)	particle diameter d_{BET} (nm)[a]	GA (%w:w)	by TGA	by EPR	by TGA (GA per nm^2)[b]	by EPR (radicals per nm^2)
SiO_2[90]-GA	96	30.3	1.7 ± 0.2	100 ± 11	101 ± 15	1.0 ± 0.2	1.0 ± 0.2
SiO_2[150]-GA	129	21.1	2.6 ± 0.2	152 ± 12	148 ± 15	1.2 ± 0.2	1.1 ± 0.2
SiO_2[300]-GA	269	10.1	4.4 ± 0.3	259 ± 18	251 ± 15	1.0 ± 0.3	1.0 ± 0.2
SiO_2[380]-GA	352	7.6	6.0 ± 0.3	366 ± 19	357 ± 15	1.1 ± 0.3	1.0 ± 0.2

[a]Estimated by d_{BET} (nm) = 6000/(2.2 (g/cm^3) × SSA (m^2/g)). [b]Estimated by dividing the GA-loading (μM/g) per SSA (m^2/g).

Table 2. Stoichiometry Ratios[a] n_{fast}, n_{slow}, and n_{total} for the Scavenging of DDPH Radicals by the SiO_2-GA NPs and Pure GA at Various Initial $[GA]_0$ Concentrations[b] for $[DDPH]_0$ = 29 μM

SiO_2[380]-GA				SiO_2[300]-GA				SiO_2[150]-GA				SiO_2[90]-GA				GA			
$[GA]_0$ (μM)	n_{fast}	n_{slow}	n_{total}	$[GA]_0$ (μM)	n_{fast}	n_{slow}	n_{total}	$[GA]_0$ (μM)	n_{fast}	n_{slow}	n_{total}	$[GA]_0$ (μM)	n_{fast}	n_{slow}	n_{total}	$[GA]_0$ (μM)	n_{fast}	n_{slow}	n_{total}
1	2.1	1.5	3.6	1	2.1	1.8	3.9	1	2.2	1.9	4.1	1	2.1	1.9	4.0	1	2.2	2.1	4.3
2	2.0	1.5	3.5	2	2.2	1.6	3.8	2	2.2	1.9	4.1	2	2.1	1.9	4.0	2	2.2	2.2	4.4
5	2.0	1.4	3.4	5	2.2	1.4	3.6	3	2.2	1.9	4.1	3	2.1	1.8	3.9	3	2.2	2.4	4.6
8	2.0	1.1	3.1	8	2.1	1.2	3.3	5	2.2	1.9	4.1	5	2.1	1.8	3.9	4	2.3	2.7	5.0
10	1.8	0.7	2.5	10	1.9	0.8	2.7	8	2.1	1.8	3.9	8	2.0	1.8	3.8	5	2.1	4.0	6.1
11	1.6	0.5	2.0	12	1.6	0.7	2.3	10	2.1	1.7	3.8	10	1.9	1.8	3.7				
14	1.2	0.4	1.7																

[a]Errors: n_{fast}, n_{slow}, n_{total} ± 0.2. [b]$[GA]_0$ ± 0.2 μM for the SiO_2-GA NPs, and ±0.1 μM for pure GA.

tyrosine-based[35] and gallic acid-based[36] phenolic radicals, via intercalation[35,36] by embedding them in the interlayer space of the clay. Moreover, GA can be grafted covalently on silica-gel and this method provides a route for the development of robust hybrid materials with a remarkable stability of the GA molecules.[37] It is noted that the grafting chemistry of GA on chitosan[30,31] was the same as on SiO_2 (i.e., GA is covalently attached by formation of a peptide bond via carboxy-group)[37] with no-impairment of the phenolic OH groups, as in other cases.[32]

Silica nanoparticles [NPs] in the commercial form of fumed silica are nowadays among the largest industrial nanotechnology products, and find applications in paints, microelectronics, pharmaceuticals, cosmetics among others.[38] Silica NPs are explored as nanocomposites for drug delivery.[39] Silica is considered biochemically inert[40] so it is vastly used as flowing-aid for nutraceutical and pharmaceutical products.[38] Nanosized SiO_2 particles with specific functionalities (e.g., antioxidant) can result in added-value hybrid nanomaterials that combine the advantages of each component. Solid inorganic particles (e.g., SiO_2) offer distinct advantages vs. organic polymer matrices, as they are far more thermally stable and chemically inert. Thus immobilizing antioxidants on NPs [nanoantioxidants] offer a unique opportunity to exploit the potential of natural antioxidants.

Here, the notion of "nano-antioxidant" is introduced with antioxidant-functionalized SiO_2 NPs and their Radical Scavenging Capacity (RSC) is investigated. More specifically, commercially available well-characterized SiO_2 NPs of various sizes (8−30 nm) are used and functionalized by covalent grafting a widely used natural antioxidant, gallic acid (GA), on their surface. The physicochemical properties of these [SiO_2-GA] nanomaterials are studied by N_2-adsorption and electron microscopy, whereas the GA attachment on the SiO_2 surface is verified by FTIR spectroscopy and thermogravimetric analysis. The radical reactions of the NPs were studied by electron paramagnetic resonance (EPR) spectroscopy. Detailed kinetic experiments were performed to assess the RSC of the SiO_2-GA NPs was quantified in comparison with pure GA based on the 2,2-diphenyl-1-picrylhydrazyl radical (DPPH$^•$) method,[41] by EPR and UV−vis spectroscopy. Their radical-induced agglomeration in solution is studied by dynamic light scattering (DLS). Specific aims of the present work are (a) to study the radical reactions, stability of the antioxidant GA molecules on the [SiO_2-GA] NPs, (b) to assess their RSC in vitro by monitoring scavenging of DPPH$^•$ radicals, (c) to assess the reusability of antioxidant NPs, and (d) to assess the effect of radical-reactions on the agglomeration state of NPs.

MATERIALS AND METHODS

Chemicals and SiO_2 NPs. 3-Aminopropyl-triethoxysilane (APTES, >98%), gallic acid monohydrate [purum >98%], and *N*-(3-dimethylaminopropyl)-*N*′-ethylcarbodiimide hydrochloride (EDC) [purum >98%], and ultrapure methanol [puriss, absolute, over molecular sieve (H_2O ≤0.01%), ≥99.5% (GC)] were obtained from Sigma-Aldrich. DPPH was obtained from Sigma-Aldrich and used within 1 month of its purchase. Four well-characterized,[42] commercially available, hydrophilic SiO_2 NPs were used (Aerosil A90, A150, and A300, A380 Evonik, formerly Degussa). Their SSA (m^2g^{-1}) determined by N_2 (PanGas, 9.9999%) adsorption at −196 °C (Micromeritics, Tristar 3000) is listed in Table 1, where the particles are labeled as "SiO_2[A]", where A is the nominal SSA given by the provider. The SiO_2 NPs had an average OH surface density[43] of 2.6−2.8 OH/nm.

Preparation of SiO_2-GA NPs. The preparation protocol[37] for the SiO_2-GA NPs employed herein was modified only with respect to the final washing. In brief, before functionalization, all SiO_2 NPs were dried at 140 °C for 12 h. Aminopropyl-SiO_2 (APTES-SiO_2) was prepared by reacting 5 g of dry SiO_2 NPs with 5 mL of APTES in 50 mL of toluene. The suspension was refluxed for 24 h at 80 °C; rinsed three times with toluene, three times with ethanol, and three times with acetone; and then dried for 18 h at 80 °C in a Buchi (B-585) rotating furnace-drier. The obtained NPs were aminopropyl-SiO_2, herein named SiO_2−NH_2 for brevity. Then, one gram of SiO_2−NH_2 was suspended in 50 mL of toluene, and GA and EDC were then added in the suspension. Covalent immobilization of GA on them was achieved by formation of amide bonds between the amine groups of

SiO_2–NH_2 and the carboxyl group of GA activated by the EDC coupler. This method was successfully applied previously on SiO_2,[37] as well as for grafting of GA on chitosan[30,31] via the carboxylate groups. For all materials, a [GA:EDC] mass ratio (3:1) was used, for example, 300 mg of GA and 100 mg of EDC per gram of SiO_2–NH_2. The mixture was refluxed for 18 h at 80 °C. Then the solid was centrifuged in a ROTINA Hettich 6000 rpm, 5 min at 25 °C and rinsed three times with toluene, three times with methanol and three times with acetone and dried at 80 °C for 12 h. Here the protocol did not involve washing in aqueous solution in the final step,[37] to avoid formation of stable GA radicals on the SiO_2-GA NPs.

Particle Characterization. The so-prepared hybrid SiO_2-GA NPs were characterized by high-resolution transmission electron microscopy (HR-TEM) on a Tecnai F30 ST. The SSA was obtained according to Brunauer-Emmet-Teller (BET) by five-point N_2 adsorption at 77 K (Micromeritics Tristar 3000). Prior to that, samples were degassed in N_2 for at least 1 h at 150 °C. The organic loading in hybrid NPs was measured by thermogravimetric (TGA) analysis performed using a Schimadzu DTG-60 analyzer. FTIR measurements were performed in KBr pellets using a PerkinElmer 580 spectrophotometer. Dynamic light scattering (DLS), Malvern Zetasizer, model Nano ZS, measurements were performed in DTS1060 folded capillary cells. The DLS conditions (concentrations of NPs and DPPH) were similar to these used for the kinetic study described in in Table 2. Several screening experiments (data not shown) showed that detectable agglomeration changes required at least 20 min of reaction, attaining a steady-state at 60 min. Thus to measure the aggregation of NPs due to the interaction with the DPPH radicals, the NPs suspension was allowed to react with DPPH for 60 min and then introduced into the DLS cell.

Dispersion of NPs. For the evaluation of the radical scavenging capacity (RSC) of the SiO_2-GA NPs, stocks were prepared by dispersing 3 mg of such NPs in 5 mL of methanol and sonicating with a total 2 kJ energy for 5 min (Sonics Vibra-cell, 40% power, 1s/1s on/off).

EPR Spectroscopy. Electron paramagnetic resonance (EPR) spectra were recorded with a Bruker ER200D spectrometer at 77K (in liquid-N_2), equipped with an Agilent 5310A frequency counter. Adequate signal-to-noise was obtained after 5–10 scans. Spin quantitation was done using DPPH as spin standard.[37] Herein, EPR spectroscopy was used as a state-of the art tool with a double purpose: (i) To determine the maximum concentration of GA molecules able to form radicals on each type of the SiO_2–NPs. This was done by oxidation of GA by O_2 in aqueous solution at alkaline pH, Figure 1.[18,19,37]

(ii) To monitor the radical reactions, for example, between DPPH and SiO_2-GA. For each SiO_2–NP, the reaction mixture consisted of SiO_2-GA nanoparticle suspension in methanol plus DPPH inside the EPR tube, (Willmad Glass Suprasil, 5.5 mm outer diameter). The initial concentrations $[DPPH:GA]_0$ were similar to those used for kinetic UV–vis experiments. To monitor the DPPH radical scavenging, we quenched the reaction at selected times from 0 to 60 min, by rapid freezing (within 10 s) the sample at 77 K. The EPR signals for DPPH:SiO_2-GA were recorded at nonsaturating microwave power 0.125 mW with a modulation amplitude of 2Gpp.[37] For comparison, similar experiments were also run for DPPH:GA.

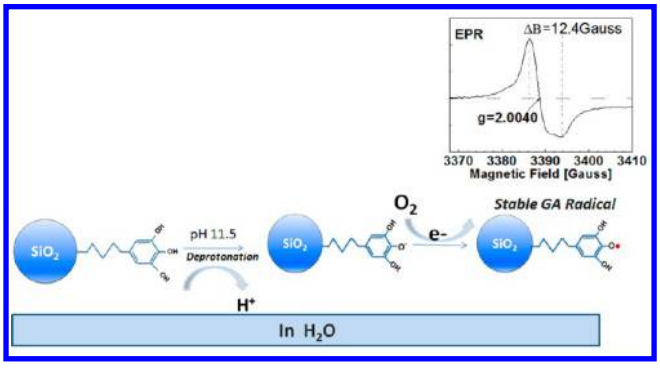

Figure 1. Formation of stable GA radicals on SiO_2-GA NPs at pH 11.5 in H_2O under oxidation by O_2.

Evaluation of the Radical Scavenging Capacity (RSC) of SiO_2-GA NPs. The RSC of the SiO_2-GA NPs was monitored using the standardized DPPH radical-method[44] which offers a suitable basis for comparative evaluation of the RSC for most natural antioxidants[41,45] as well as GA-functionalized polymers.[30−32] Here, 25–50 μL of SiO_2-GA NPs stock suspensions in methanol and 3 mL of methanolic solution of DPPH (29×10^{-6} M) were mixed inside 1 cm quartz cuvettes (Hellma suprasil quartzglass, 100-QS). For each SiO_2-GA sample, at least five kinetic experiments were run corresponding to five GA molar-concentrations from 1 to 14×10^{-6} M (Table 2). The final GA concentration was calculated based on the GA-loading of each material (Table 1). Absorbance measurements started immediately. The decrease in absorbance at 515 nm was determined continuously with data acquisition at 2 s intervals by a Varian, Cary 500 spectrophotometer. For comparison, similar kinetic experiments were also performed for DPPH interacting with pure GA. All determinations were performed in duplicate. Control EPR and UV–vis measurements showed that the nonfunctionalized SiO_2 NPs, at concentrations used in the present kinetic experiments, for example, several micrograms of SiO_2 in 3 mL, had a negligible effect on the concentration of DPPH radicals.

RESULTS

Characterization of SiO_2-GA NPs. After the SiO_2 surface functionalization with GA, the color of NPs was converted from pristine-white (Figure 2a) to faint-yellow (Figure 2b). In methanolic solution, these particles resulted in a stable opaque suspension (Figure 2c). This minimal color change is important as it indicates that such hybrid NPs will induce minor, if any, sensory changes in commercial products that employ them (e.g., in cosmetics, food, medicine, etc.).

Figure 2. (a) Untreated and (b) functionalized SiO_2[90]-GA NPs. (c) Suspension (5 mg of SiO_2[90]-GA NPs in 10 mL of methanol).

Figure 3 shows HR-TEM images of the SiO_2[90] NPs before (a) and after (b) GA functionalization, verifying that the treatment has not altered the NPs that keep their rather corrugated structure, in agreement with the literature.[42]

The amount of GA immobilized on SiO_2 nanoparticles determined by TGA are listed in Table 1.

The surface density of the GA on all SiO_2 NPs was about 1 GA per nm^2. As verified by EPR, this surface density is beneficial because it prohibits GA-GA radical–radical couplings, which would inhibit the DPPH-radical scavenging activity of the NPs.

FTIR Spectroscopy. Figure 4 shows representative FTIR spectra for SiO_2[90] and SiO_2[90]-GA NPs. The spectrum for pure GA in KBr is also included for comparison. The 3500–3280 cm^{-1} peaks in the FTIR spectrum of SiO_2-GA are assigned to OH groups of GA.[37] Similarly the 1543, 1430, and 1385 cm^{-1} are attributed to C=C stretching and aliphatic CH bending vibrations of GA. However, the spectral features of SiO_2-GA in the region 1710–1600 cm^{-1} present changes

dx.doi.org/10.1021/am301751s | ACS Appl. Mater. Interfaces 2012, 4, 6609–6617

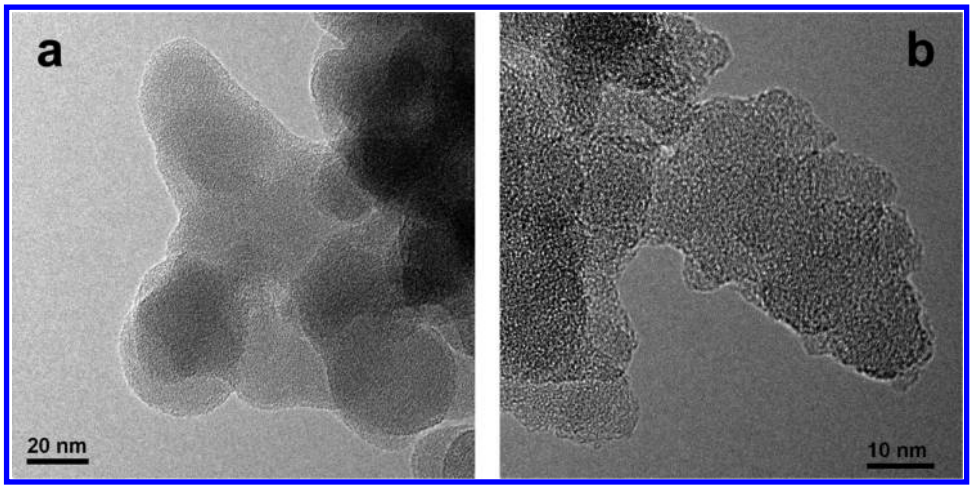

Figure 3. HR-TEM image of SiO_2[90] NPs, (a) before and (b) after GA surface functionalization.

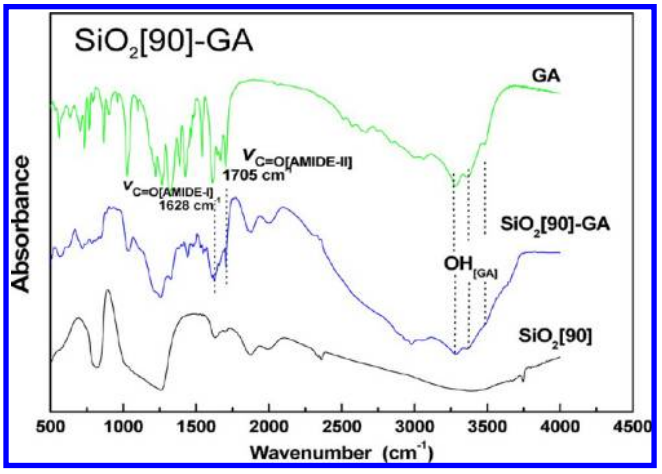

Figure 4. FTIR spectra of SiO_2[90] (black line), and SiO_2[90]-GA functionalized nanoparticles (blue line). The FTIR spectrum of GA is included for comparison (green line).

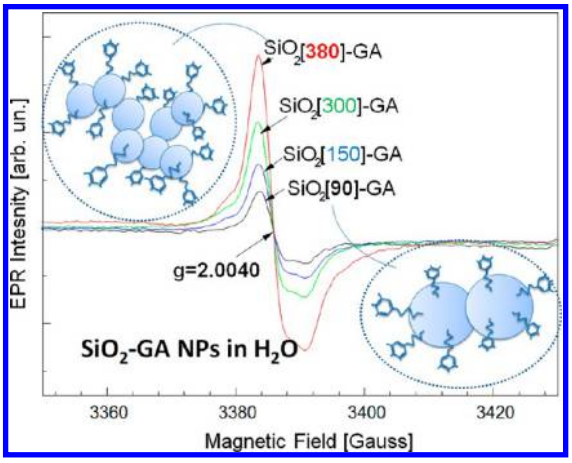

Figure 5. EPR spectra for 20 mg of SiO_2-GA in H_2O solution at pH 11.5. The smaller particles such as SiO_2[380]-GA have higher loading of GA per gram than the larger particles such as SiO_2[90]-GA. However, the average surface density of GA molecules is similar in all particles.

compared with those of GA. That is, the peak at 1708 cm^{-1} attributed to the C═O stretch of the carboxyl group, shifts at 1706 cm^{-1} and a new broad band at 1628 cm^{-1} appears in SiO_2-GA.

These peaks are attributed to ν(C═O) (amide I) and ν(C−N) (amide II) vibrations indicating the formed peptide bond the NH_2 of aminopropyl and the carboxylate of GA.[30,37] This is key proof for the covalent attachment of GA on the SiO_2 particles.[37] The FTIR spectra for the other NPs verify the covalent attachment of GA on the SiO_2[150], SiO_2[300] and SiO_2[380] NPs (please see Figure S1 in the Supporting Information).

EPR Characterization. Figure 5 shows EPR spectra for 20 mg of all SiO_2-GA NPs in H_2O (pH 11.5). The radical-signal intensity follows the GA surface-loading trend. More precisely, the spin quantitation data (please see Table 1) show that the concentration of the GA radicals, estimated by EPR, is quite comparable to the concentration of the GA molecules, estimated by TGA, listed in Table 1.

This means that practically all the grafted GA molecules are capable of forming radicals; in other words, all grafted GA molecules are capable of participating in radical scavenging reactions.

The g-factor is a sensitive index of the unpaired-electron distribution on the GA molecule.[18,19] As we have demonstrated recently, using High Field 285 GHz EPR spectroscopy[18] the *g*-value 2.0040 is characteristic of the unpaired electron localized mainly in the three phenolic-ring oxygens of the GA molecule.[18] Accordingly, the *g*-values for the GA radicals on the SiO_2-GA particles (see Figure 5) g = 2.0040 show that on the grafted GA molecules, the radicals are localized on the phenolic-ring oxygens. This is of immediate relevance for the antioxidant activity that we discuss in the following, because this renders the phenolic oxygens highly reactive sites on GA, favoring the fast-radical movement via the HAT mechanism to DPPH (Figure 8a,b).

DPPH-Radical Scavenging. *a. EPR and UV−Vis Spectra.* The interaction of the SiO_2-GA NPs with DPPH radicals resulted in fast decoloration of the DPPH solution (Figure 6a). The initial purple color is the well-known characteristic for the DPPH radicals in methanol[41,44−46] corresponding to the UV−vis spectrum with a maximum at 515 nm (Figure 6b). The EPR spectrum [red line] in Figure 6c is typical for DPPH-radicals in methanol.[30] This EPR signal decayed at a rate comparable with the UV−vis kinetics (Figure 6b) and this provides solid evidence that the spectral changes observed in

dx.doi.org/10.1021/am301751s | ACS Appl. Mater. Interfaces 2012, 4, 6609−6617

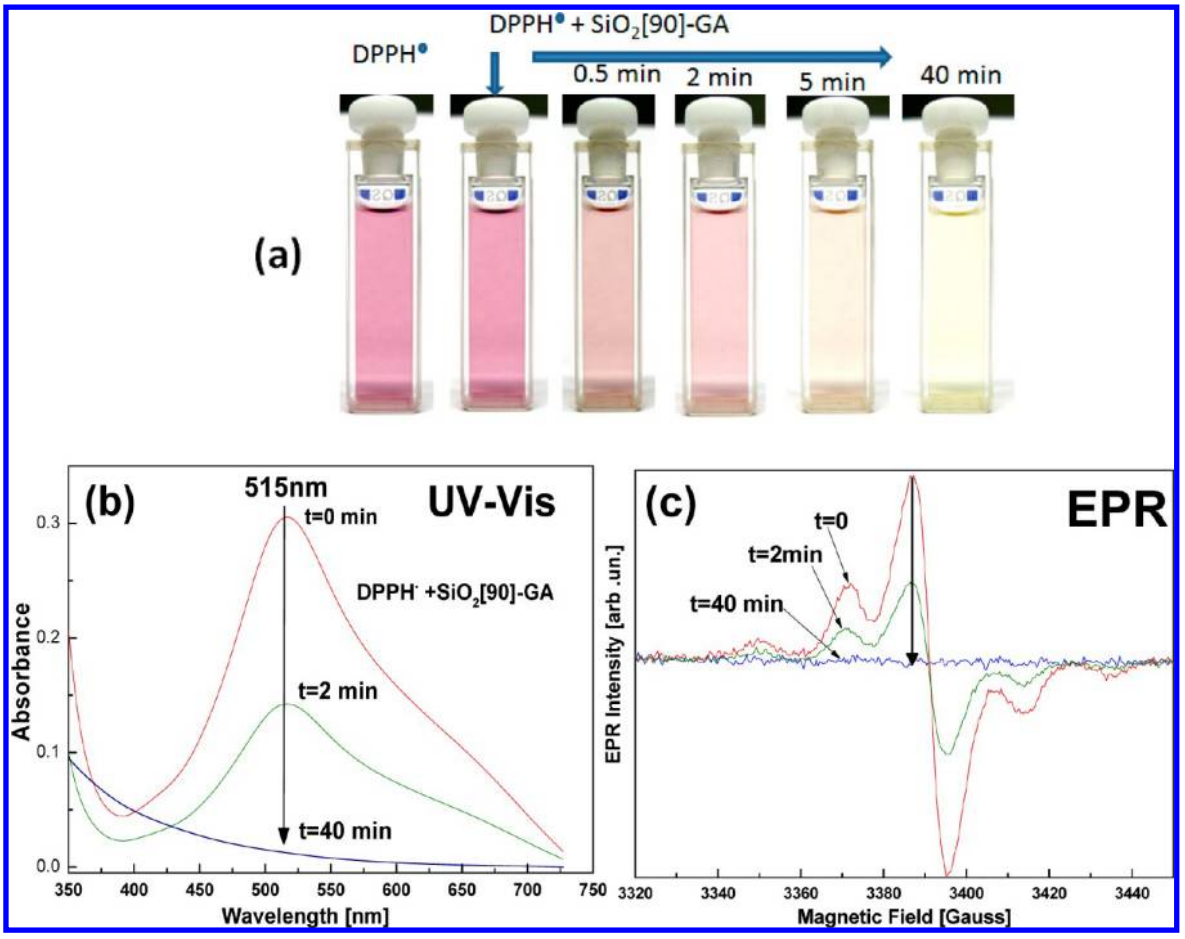

Figure 6. (a) Decolorization of the DPPH radicals in methanol reacting SiO_2[90]-GA NPs. (b) Time-decay of UV−vis absorption and (c) the EPR signal the DPPH-radical radicals interacting with SiO_2[90]-GA NPs in methanol.

DPPH:SiO_2[90]-GA are exclusively due to scavenging of DPPH radicals. Any other route not involving radical scavenging, for exampoe, surface adsorption of DPPH on the NPs, would not result in decay of the EPR signal as observed in Figure 6c.

It is well-established that the kinetics of DPPH scavenging can provide (i) quantitative information on the RSC of antioxidants,[41,44−46] and [ii] mechanistic insights on the underlying physicochemical events.[41,44−46] Thus, the decay of visible absorbance at 515 nm was used for the quantitative analysis of the DPPH-radical scavenging kinetics.[41,44−46]

b. Kinetics. Figure 7a displays kinetic traces recorded for each type of NPs for initial GA concentrations $[GA]_0 = 2.0\ \mu M$. For comparison, the decay trace recorded for 2.0 μM of pure GA is also shown. The full kinetic data sets for all NPs at other initial GA concentrations studied herein are provided in Figure S2 of the Supporting Information. In Figure 8a, we mark the two kinetic regions observed for pure GA as well as for the SiO_2-GA NPs: (i) fast kinetic phases for reaction times below 1 min, and (ii) slow decay phases persisting at prolonged times.

Method for Analysis of Kinetic Data. For DPPH:GA the mixed-phase decay is well-documented[41,44−46] and can be operationally analyzed based on fast and slowreactions.

Fast-DPPH Decay Reactions. The initial fast decay of the DPPH radical (DPPH•) interacting with a phenolic antioxidant (ArOH)[41,44−46] is due to rapid reactions 1 and 2

$$ArOH + DPPH^{\bullet} \rightarrow ArO^{\bullet} + H - DPPH \quad (1)$$

$$ArO^{\bullet} + DPPH^{\bullet} \rightarrow ArO - quinone \quad (2)$$

These are H-Atom Transfer reactions [HAT] from the phenolic OH groups to the DPPH-radical.[45−48] For the case of our SiO_2-GA NPs, reaction 1 corresponds to the HAT from one OH of the GA molecule to one DPPH-radical, as depicted in Figure 8a. Accordingly, a GA semiquinone radical is formed. This is a short-lived species because, according to reaction 2, it can react rapidly with a second DPPH-radical to produce a GA-quinone, which is a nonradical product, as depicted in Figure 8b.

Slow-DPPH Decay Reactions. The slow-decay phases resolved for [DPPH:SiO_2-GA] may involve radical−radical dimerization/polymerization reaction such as that described in reaction 3

$$GA^{\bullet} + DPPH^{\bullet} \rightarrow [GA - DPPH] \quad (3)$$

Recent credible experimental data, using NMR[47] or mass spectrometry[48] show that rather multiple reactions involving covalent adducts between the DPPH and the polyphenol radical as described in reaction 3 take place during the secondary slow-phase. Herein, fitting by simple exponential decays allows a quantitative estimate of the number of DPPH radicals reacting with the GA molecules as well as an estimate of the apparent kinetic time-scale.

The total scavenged DPPH radicals can be estimated by

$$[DPPH]_{total\ scavenged} = [DPPH]_0 - [DPPH]_{remain} \quad (4)$$

dx.doi.org/10.1021/am301751s | ACS Appl. Mater. Interfaces 2012, 4, 6609−6617

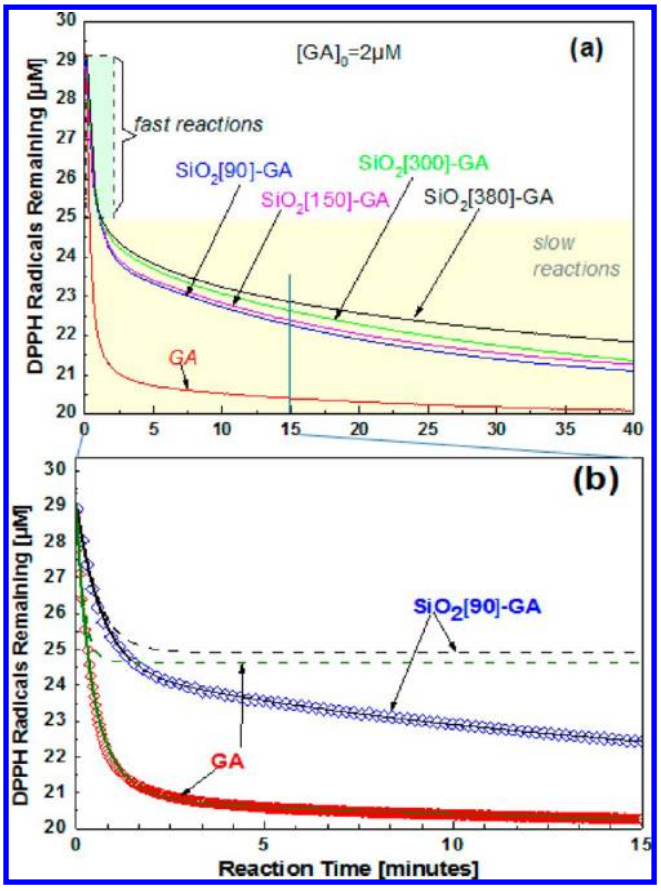

Figure 7. (a) Kinetics of decay of absorbance at 515 nm for DPPH radicals ($[DPPH]_0 = 29.0 \pm 0.1\ \mu M$) reacting with SiO_2-GA NPs. (b) [solid lines] theoretical fit for the DPPH:SiO_2-GA (black) and DPPH:GA (green) data. The experimental data shown by [◊] for pure GA (red) and SiO_2[90]-GA (blue), are zoomed at the 0−15 min for better viewing the initial phases. [dashed lines] theoretical fast exponential components for the DPPH:SiO_2-GA (black) and DPPH:GA (green) data.

where $[DPPH]_{remain}$ can be estimated by the kinetics plot after completion of the reaction or by nonlinear fitting of the kinetic traces by an exponential decay function.

From these data the total stoichiometry of the reaction n_{total} can be defined as

$$n_{total} = \frac{DPPH_{total\ scavenged}}{[GA]_0} \quad (5a)$$

where $[GA]_0$ = moles of GA in the initial reaction mixture.

In our work, of key importance was the quantitative estimation of the contribution of the fast and slow kinetics to the total stoichiometry. Thus, we define a stoichiometry ratio, n_{fast} as

$$n_{fast} = \frac{\text{moles of DPPH radicals scavenged via HAT reactions}}{[GA]_0} \quad (5b)$$

Reactions 1 and 2 set an upper limit for $n_{fast} = 2$. Previous reports for the DPPH:GA[41,44−46] use this stoichiometry ratio as evidence for the occurrence of the rapid HAT mechanism.

A stoichiometry ratio for the slow reactions can be defined similarly as

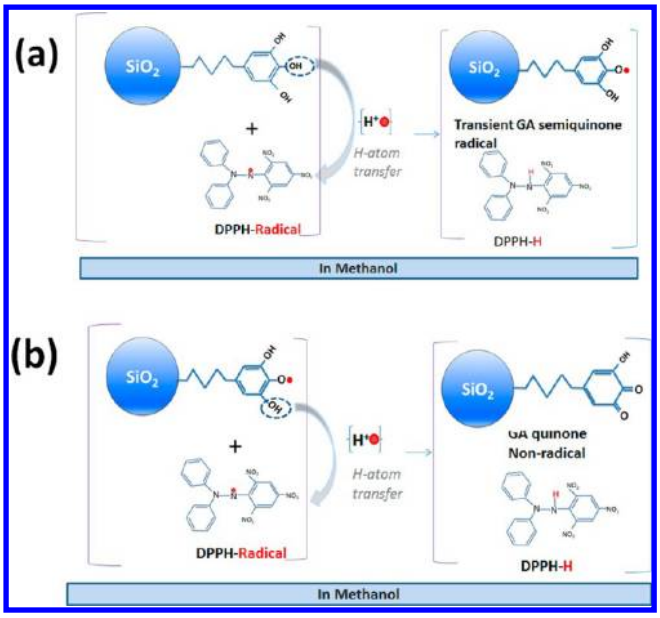

Figure 8. (a) Scavenging of one DPPH radical by SiO_2-GA NPs via hydrogen-atom transfer [HAT] from the GA molecule forming a transient GA radical. (b) Scavenging of a second DPPH radical by SiO_2-GA NPs via hydrogen-atom transfer [HAT] from the GA semiquinone forming a nonradical GA quinone.

$$n_{slow} = \frac{\text{moles of DPPH radicals scavenged via secondary reactions}}{[GA]_0} \quad (5c)$$

In DPPH:GA these secondary reactions can account for up to $n_{slow} = 4$ DPPH radicals scavenged per GA molecule.[41,44,46]

The n_{fast} and n_{slow} as well as the total stoichiometry n_{total} of the reaction are additive

$$n_{total} = n_{fast} + n_{slow} \quad ([6])$$

As shown previously for heterogeneous nanocatalytic systems,[49] the kinetic constants of the slow phases reflect only the slower steps, which are influenced by the mobility, diffusion, aggregation, and particle−particle interaction of the NPs themselves.[43,46,49] In this context, analysis of the kinetic times is a rather complex task which was beyond the scope of the present work. Instead, herein we focused exclusively on the analysis of the stoichiometry ratios.

Figure 7b (solid lines) shows theoretical exponential-decay fitting for SiO_2[90]-GA (Figure 7b, green line) as well as for pure GA(Figure 7b, black line). Symbols (◊) are the corresponding experimental data. To facilitate the data analysis, the fast-decay exponential components are also presented by the dashed lines in Figure 7b.

Stoichiometry Ratios of Fast Reactions n_{fast}. Upon interaction with the SiO_2-GA NPs, a significant fraction of the DPPH radicals are rapidly scavenged, and see initial fast decay observed for all NPs, Figure 7a,b and Figure S2 in the Supporting Information. According to the fit (Figure 7b dashed line black) during this fast kinetic phase the SiO_2 [90]-GA NPs had scavenged $4.1(\pm 0.2)\ \mu M$ of DPPH radicals. By dividing this with the initial $[GA]_0 = 2.0(\pm 0.2)\mu M$ according to eq [5b], we estimate a stoichiometry ratio $n_{fast} = 2.1 \pm 0.2$, listed in Table 2. In a similar manner, the scavenging yield of the fast

dx.doi.org/10.1021/am301751s | ACS Appl. Mater. Interfaces 2012, 4, 6609−6617

component of pure GA (Figure 7b, black dashed line) was 4.3(±0.2) μM which gives n_{fast} = 2.2 ± 0.2, listed in Table 2.

This is in agreement with previous reports for n_{fast} values for pure GA[43,46−48] for $[GA]_0 \ll [DPPH]_0$, under second-order kinetics.[45,46] The stoichiometry ratios n_{fast} for all NPs calculated using the kinetics presented in Figure S2 in the Supporting Information are listed in Table 2, and plotted vs $[GA]_0$ in Figure 9a.

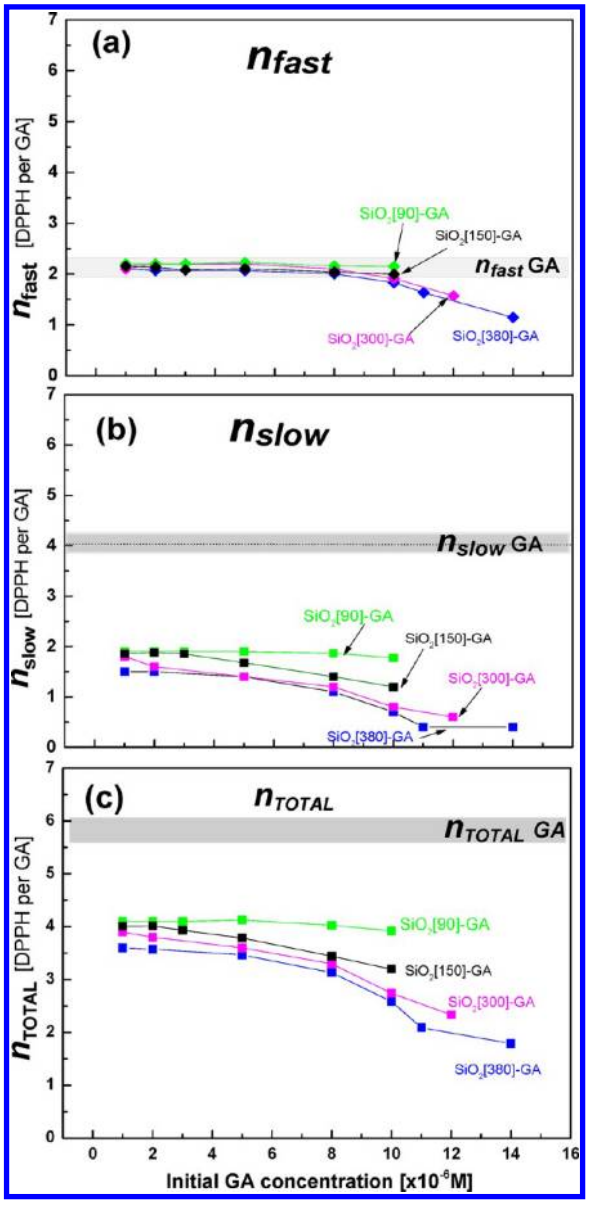

Figure 9. Plot of stoichiometry ratios (a) n_{fast}, (b) n_{slow}, and (c) n_{total} vs initial $[GA]_0$ concentration for the SiO_2-GA NPs in methanolic solution. The corresponding maximum n values for pure gallic acid are displayed by the horizontal gray bars.

Total- and Slow-Phase Stoichiometry Ratios. The total DPPH radicals scavenged by the SiO_2-GA NPs are listed in Table 2, and plotted vs $[GA]_0$ in Figure 9c. For $[GA]_0$ = 2 μM, n_{total} for SiO_2[90]-GA was 4.0 and n_{total} = 3.5 for SiO_2[380]-GA, whereas for $[GA]_0$ = 10 μM, n_{total} (SiO_2[90]-GA) = 3.7 and n_{total}(SiO_2[380]-GA) = 2.5. At higher $[GA]_0$ concentrations, differences in n_{total} values become evident, as seen in Figure 9c. The origin of these differences can be understood by referring to Figure 7a, for example, for $[GA]_0$ = 2 μM, where at prolonged reaction times, relatively fewer DPPH radicals are scavenged by NPs with higher SSA. Figure 9c clearly depicts this trend of larger NPs (lower-SSA) showing a smaller decline in their n_{total}. For example, SiO_2[90]-GA showed less than 20% decrease of n_{total} at $[GA]_0$ = 10 μM.

Overall, the observed decline of the n_{total} for higher SSA NPs at increased $[GA]_0$ indicate that an inhibitory mechanism exists that depends (i) on the SSA of the NPs and [ii] the initial concentration $[GA]_0$. Importantly, the data for n_{fast}, Figure 9a, show that this mechanism has a lower impact on the fast reactions, thus the decline of the n_{total} data at high $[GA]_0$ must be related mostly with the slow reactions. Figure 9b shows a significant dependence of the n_{slow}(i) on SSA and, (ii) on $[GA]_0$. For example, the SiO_2[380]-GA showed n_{slow} = 1.5 for $[GA]_0$ = 1 μM and n_{slow} = 0.4 for $[GA]_0$ > 10 μM, whereas the SiO_2[90]-GA showed n_{slow} = 1.9 and 1.8 respectively. This contrasting behavior of n_{fast} and n_{slow} implies that complex inhibitory reactions take place after the first minutes where the fast reactions have been accomplished. At increasing $[GA]_0$, the secondary-slow reactions eventually result in a severe inhibition of DPPH$^{\bullet}$ scavenging by high SSA NPs, as manifested by the trend

$$n_{slow}: SiO_2[90]-GA > SiO_2[150]-GA > SiO_2[300]-GA > SiO_2[380]-GA$$

In the following, in an effort to shed light on the possible factors that inhibit the RSC at increasing $[GA]_0$, we have used DLS to study in more detail the aggregation dynamics of the NPs during their interaction with DPPH radicals.

Radical-Induced Agglomeration of High-SSA NPs. The DLS data (Figure 10a) indicate that after their interaction with DPPH-radicals the high-SSA SiO_2[380]-GA NPs undergo a dramatic agglomeration. As shown in Figure 10b at the higher mass-concentrations tested herein, e.g., 30 mg/L (corresponding to $[GA]_0$ = 10 μM), the average size of the SiO_2[380]-GA agglomerates approaches 1 μm, after DPPH-induced agglomeration.

This is a ~6-fold increase of the agglomerate size of the SiO_2[380]-GA NPs, compared to 180 nm in the absence of DPPH-radicals (Figure 10a). The NPs did not agglomerate in the absence of DPPH radicals (open symbols in Figure 10b). Remarkably, the lower SSA [larger average diameter] SiO_2[90]-GA NPs showed only a limited increase in their agglomerate size, from 130 to 240 nm, after interaction with DPPH; compare solid vs open red symbols in Figure 10b. Moreover, it is underlined that to achieve the same $[GA]_0$ concentration a 3.4-fold higher mass-concentration has been used for the SiO_2[90]-GA NPs vs the SiO_2[380]-GA NPs, see top-*X*-axis in Figure 10b. Thus the SiO_2[380]-GA NPs agglomerate to a significantly higher degree than the SiO_2[90]-GA NPs despite their significantly lower mass-concentration.

Reusability of the Antioxidant NPs. The reusability of SiO_2[90]-GA NPs was evaluated after their interaction with DPPH radicals as follows: SiO_2[90]-GA NPs were allowed to react with DPPH at two $[DPPH]_0$:$[GA]_0$ mole ratios, [29 μM:2 μM] and [29 μM:10 μM]. Within 40 min, the solution was fully decolorized, as in Figure 7a. The particles, after washing (x3 with methanol), did not change color and were

dx.doi.org/10.1021/am301751s | ACS Appl. Mater. Interfaces 2012, 4, 6609−6617

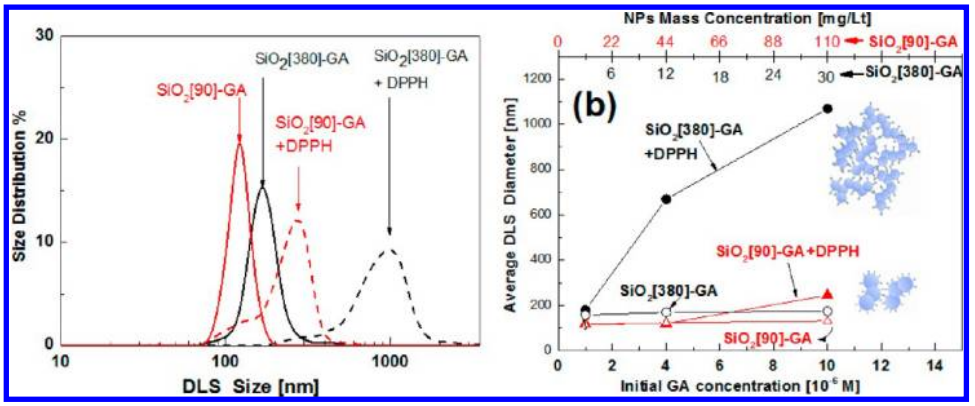

Figure 10. (a) Dynamic light scattering size distributions of SiO_2[90]-GA (red lines) and SiO_2[380]-GA NPs (black lines), before (solid lines) and after (dashed lines) their interaction with DPPH radicals ($[DPPH]_0$ = 29 μM) for 60 min. The NPs mass-concentrations corresponded to $[GA]_0$ = 10 μM. (b) Average DLS diameter vs initial GA-concentration (lower *X*-axis) or mass-concentration of NPs (top *X*-axis). Solid symbols (●,▲) NPs interacting with DPPH, open symbols (○, Δ) NPs without DPPH. Note that to achieve the same GA concentration [based on the GA-loadings] much higher mass concentration has been used for the SiO_2[90]-GA NPs than for SiO_2[380]-GA NPs.

easily redispersed in methanol. At $[GA]_0$ = 2 μM as well as at $[GA]_0$ = 10 μM, the DPPH scavenging kinetics were comparable for the reused as for the unused NPs. This shows that under these conditions the NPs are reusable and their RSC has not been impaired after interaction with the DPPH radicals.

DISCUSSION

The present work shows that silica particles offer a versatile scaffold to develop highly efficient antioxidant SiO_2-GA hybrid nanomaterials, by covalent grafting of GA antioxidant molecules. The so engineered low-cost SiO_2-GA nanoantioxidant materials are capable to scavenge DPPH radicals via fast H-Atom Transfer reactions. The present data show that during the fast reactions the SiO_2-GA NPs are capable to scavenge 2 DPPH radicals per GA molecule. This is among the most important findings of the present work since it shows that surface-grafted GA molecules on the SiO_2 NPs are capable of performing fast H-atoms reactions toward DPPH radicals. To the best of our knowledge, this provides the first proof-of-concept for RSC via HAT reactions by a nanoantioxidant material. Moreover, the NPs are reusable and their RSC has not been impaired after interaction with the DPPH radicals. This opens opportunities for applications where low-cost, stable antioxidants are needed, such as food, polymers, cosmetics, etc.

Moreover, the present study provides a wealth of new information on basic physicochemical mechanism involved in their radical scavenging activity. The SiO_2-GA NPs can perform two types of radical scavenging reactions: (i) rapid HAT reactions and (ii) secondary/slow radical−radical coupling reactions. The DLS data revealed a novel phenomenon, significant radical-induced agglomeration of high-SSA SiO_2-GA NPs taking place during the secondary reactions.

On the basis of the DLS data, a mechanism can be postulated explaining the observed quenching of the slow reactions (and the ensuing decline of n_{slow} at increased SSA and $[GA]_0$ Figure 9b) as follows: at increasing $[GA]_0$ the higher-SSA NPs tend to agglomerate during their secondary reactions with DPPH radicals. These agglomeration reactions are expected to be slow and diffusion-limited since they would involve particle−particle encounters and radical−radical coupling events. Thus agglomeration events are triggered only after completion of the fast HAT reactions. Otherwise stated, the initial fast HAT reactions are not inhibited by the radical-induced agglomeration, thus explaining the relatively minimal decline of n_{fast} in Figure 9a.

In real systems of pertinence to the present study such as foods, biological systems, etc., the local concentration of radicals and antioxidants is expected to be below the lower concentrations of the present experiments. Under these conditions, agglomeration effects should not be expected and all SiO_2-GA NPs will behave in the same way regardless of their SSA. Moreover, in applications of antioxidants, such as food technology, biological systems, medicine, these secondary reactions might be nondesirable,[47,48] because they might result in uncontrolled/undesirable by-products, such as those resolved by NMR and mass spectrometry for DPPH:GA.[47,48] Thus the nonoccurrence or inhibition of the secondary reactions can be considered as beneficial from an application/engineering point of view.

Within another context, a radical-induced NP agglomeration mechanism has been reported by Weissleder et al.,[50−52] for magnetic Fe-oxide-NPs[52] functionalized with tyrosyl radical-forming moieties. There[50−52] NP-agglomeration was triggered by radicals generated via an enzymatic reaction.[50−52] Here, NP agglomeration can be controlled by SSA and particle size.

CONCLUSIONS

Silica particles offer a versatile scaffold to develop highly efficient antioxidant SiO_2-GA hybrid nanomaterials, by covalent grafting of GA antioxidant molecules. Here, a first proof-of-concept of engineered low-cost nanoantioxidant materials capable to scavenge DPPH radicals via fast H-atom transfer reactions is presented. All SiO_2 NPs perform fast HAT reactions at stoichiometry ratios n_{fast} = 2 comparable to that of pure GA. Additional, secondary/slow DPPH radical scavenging reactions are also performed by these nanoantioxidants. Potential applications of the novel nanoantioxidant materials can be envisaged in cases where low-cost, stable antioxidants are needed, for example, food, polymers, cosmetics etc. A novel phenomenon has been observed in radical-induced agglomeration of high SSA NPs, which takes place during the secondary slow reactions. This radical-induced agglomeration can be used to inhibit the secondary reactions in a controlled manner by varying the primary particle size and/or the initial $[GA]_0$.

Grafting of active organic moieties such as antioxidants on SiO_2 nanoparticles prevents their deterioration. After their interaction with DPPH radicals, the nanoantioixdant particles can be reused by a simple washing, with no impairment of their RSC.

■ ASSOCIATED CONTENT

Supporting Information

Figure S1 FTIR Spectra for GA, SiO_2[150]-GA, SiO_2[300]-GA, SiO_2[380]-GA, and pure GA. Figure S2 Kinetic DPPH··-decay data for SiO_2[90]-GA, SiO_2[150]-GA, SiO_2[300]-GA, SiO_2[380]-GA NPs, and pure GA. This material is available free of charge via the Internet at http://pubs.acs.org/

■ AUTHOR INFORMATION

Corresponding Author

*E-mail: deligiannakis@ptl.mavt.ethz.ch.

Notes

The authors declare no competing financial interest.

†Visiting Professor, on sabbatical leave from the Department of Environmental and Natural Resources Management, University of Western Greece, Seferi 2, 30100 Agrinio, Greece.

■ ACKNOWLEDGMENTS

We kindly acknowledge financial support from the Swiss National Science Foundation (Grant 200020-126694) and the European Research Council.

■ REFERENCES

(1) Halliwell, B. *Annu. Rev. Nutr.* **1996**, *16*, 33−50.
(2) Aruoma, O. I. *J. Am. Oil Chem. Soc.* **1998**, *75*, 199−212.
(3) Balasundram, N.; Sundram, K.; Samman, S. *Food Chem.* **2006**, *99*, 191−203.
(4) Al-Malaika, S. In *Plastic Additives*; Pritchard, G., Ed.; Chapman and Hall: London, 1998; p 56.
(5) Moure, A.; Cruz, J. M.; Franco, D.; Dominguez, J. M.; Sineiro, J.; Dominguez, H.; Nunez, M. J.; Parajo, J. C. *Food Chem.* **2001**, *72*, 145−171.
(6) Hirano, R.; Sasamoto, W.; Matsumoto, A.; Itakura, H.; Igarashi, O.; Kondo, K. *J. Nutr. Sci. Vitaminol.* **2001**, *47*, 357−362.
(7) RiceEvans, C. A.; Miller, J.; Paganga, G. *Trends Plant Sci.* **1997**, *2*, 152−159.
(8) Stratil, P.; Klejdus, B.; Kuban, V. *J. Agric. Food Chem.* **2006**, *54*, 607−616.
(9) Becker, L. *Int. J. Toxicol.* **2007**, *26*, 89−118.
(10) Lu, Z. B.; Nie, G. J.; Belton, P. S.; Tang, H. R.; Zhao, B. L. *Neurochem. Int.* **2006**, *48*, 263−274.
(11) Dwibedy, P.; Dey, G. R.; Naik, D. B.; Kishore, K.; Moorthy, P. N. *Phys. Chem. Chem. Phys.* **1999**, *1*, 1915−1918.
(12) Saeki, K.; Yuo, A.; Isemura, M.; Abe, I.; Seki, T.; Noguchi, H. *Biol. Pharm. Bull.* **2000**, *23*, 1391−1394.
(13) Sakaguchi, N.; Inoue, M.; Isuzugawa, K.; Ogihara, Y.; Hosaka, K. *Biol. Pharm. Bull.* **1999**, *22*, 471−475.
(14) Serrano, A.; Palacios, C.; Roy, G.; Cespon, C.; Villar, M. L.; Nocito, M.; Gonzalez-Porque, P. *Arch. Biochem. Biophys.* **1998**, *350*, 49−54.
(15) Sakaguchi, N.; Inoue, M.; Ogihara, Y. *Biochem. Pharmacol.* **1998**, *55*, 1973−1981.
(16) Inoue, M.; Sakaguchi, N.; Isuzugawa, K.; Tani, H.; Ogihara, Y. *Biol. Pharm. Bull.* **2000**, *23*, 1153−1157.
(17) Sohi, K. K.; Mittal, N.; Hundal, M. K.; Khanduja, K. L. *J. Nutr. Sci. Vitaminol.* **2003**, *49*, 221−227.
(18) Christoforidis, K. C.; Un, S.; Deligiannakis, Y. *Environ. Sci. Technol.* **2010**, *44*, 7011−7016.
(19) Giannakopoulos, E.; Christoforidis, K. C.; Tsipis, A.; Jerzykiewicz, M.; Deligiannakis, Y. *J. Phys. Chem. A* **2005**, *109*, 2223−2232.
(20) Giannakopoulos, E.; Deligiannakis, Y. *Langmuir* **2007**, *23*, 2453−2462.
(21) Talcott, S. T.; Howard, L. R. *J. Agric. Food Chem.* **1999**, *47*, 2109−2115.
(22) Pan, J. Q.; Lau, W. W. Y.; Lin, J.; Tan, K. L.; Goh, S. H. *Polym. Degrad. Stab.* **1995**, *49*, 231−237.
(23) Drosos, M.; Jerzykiewicz, M.; Louloudi, M.; Deligiannakis, Y. *Colloid Surf., A* **2011**, *389*, 254−265.
(24) Haider, N.; Karlsson, S. *Polym. Degrad. Stab.* **1999**, *64*, 321−328.
(25) Scoponi, M.; Cimmino, S.; Kaci, M. *Polymer* **2000**, *41*, 7969−7980.
(26) Scott, G.; Islam, S. *Polym. Degrad. Stab.* **1999**, *63*, 61−64.
(27) Allen, N. S.; Zeynalov, E. B.; Sanchez, K. D.; Edge, M.; Kabetkina, Y. P.; Johnson, B. *J. Vinyl Addit. Technol.* **2010**, *16*, 1−14.
(28) Debus, R. J. *Biochim. Biophys. Acta* **1992**, *1102*, 269−352.
(29) Rex, R. W. *Nature* **1960**, *188*, 1185−1186.
(30) Pasanphan, W.; Buettner, G. R.; Chirachanchai, S. *J. Appl. Polym. Sci.* **2008**, *109*, 38−46.
(31) Cho, Y. S.; Kim, S. K.; Ahn, C. B.; Je, J. Y. *Carbohydr. Polym.* **2011**, *83*, 1617−1622.
(32) Cirillo, G.; Kraemer, K.; Fuessel, S.; Puoci, F.; Curcio, M.; Spizzirri, U. G.; Altimari, I.; Iemma, F. *Biomacromolecules* **2010**, *11*, 3309−3315.
(33) Aytekin, A. O.; Morimura, S.; Kida, K. *J. Biosci. Bioeng.* **2011**, *111*, 212−216.
(34) Arrua, D.; Strumia, M. C.; Nazareno, M. A. *J. Agric. Food Chem.* **2010**, *58*, 9228−9234.
(35) Gournis, D.; Deligiannakis, Y.; Karakassides, M. A.; Boussac, A.; Ioannidis, N.; Petridis, D. *Langmuir* **2002**, *18*, 10024−10029.
(36) Giannakopoulos, E.; Stathi, P.; Dimos, K.; Gournis, D.; Sanakis, Y.; Deligiannakis, Y. *Langmuir* **2006**, *22*, 6863−6873.
(37) Stathi, P.; Louloudi, M.; Deligiannakis, Y. *Chem. Phys. Lett.* **2009**, *472*, 85−89.
(38) Pratsinis, S. E. In *History of Manufacture of Fine Particles in High-Temperature Aerosol Reactors*; Ensor, D. S., Lohr, K. N., Eds.; RTI Press: Research Triangle Park, NC, 2011; Chapter 18, pp 475−507.
(39) Vallet-Regi, M.; Balas, F.; Arcos, D. *Angew. Chem., Int. Ed.* **2007**, *46*, 7548−7558.
(40) Brunner, T. J.; Wick, P.; Manser, P.; Spohn, P.; Grass, R. N.; Limbach, L. K.; Bruinink, A.; Stark, W. J. *Environ. Sci. Technol.* **2006**, *40*, 4374−4381.
(41) Mishra, K.; Ojha, H.; Chaudhury, N. K. *Food Chem.* **2012**, *130*, 1036−1043.
(42) Camenzind, A.; Schweizer, T.; Sztucki, M.; Pratsinis, S. E. *Polymer* **2010**, *51*, 1796−1804.
(43) Mueller, R.; Kammler, H. K.; Wegner, K.; Pratsinis, S. E. *Langmuir* **2003**, *19*, 160−165.
(44) Brand-Williams, W.; Cuvelier, M. E.; Berset, C. *LWT-Food Sci. Technol.* **1995**, *28*, 25−30.
(45) Sanchez-Moreno, C. *Food Sci. Technol. Int.* **2002**, *8*, 121−137.
(46) Goupy, P.; Dufour, C.; Loonis, M.; Dangles, O. *J. Agric. Food Chem.* **2003**, *51*, 615−622.
(47) Sawai, Y.; Moon, J. H. *J. Agric. Food Chem.* **2000**, *48*, 6247−6253.
(48) Osman, A. M. *Biochem. Biophys. Res. Commun.* **2011**, *412*, 473−478.
(49) Jia, H. F.; Zhu, G. Y.; Wang, P. *Biotechnol. Bioeng.* **2003**, *84*, 406−414.
(50) Bogdanov, A.; Matuszewski, L.; Bremer, C.; Petrovsky, A.; Weissleder, R. *Mol. Imaging* **2002**, *1*, 16−23.
(51) Perez, J. M.; Simeone, F. J.; Tsourkas, A.; Josephson, L.; Weissleder, R. *Nano Lett.* **2004**, *4*, 119−122.
(52) Tassa, C.; Shaw, S. Y.; Weissleder, R. *Acc. Chem. Rev.* **2011**, *44*, 842−852.